

## Supporting Information

# Molecular Engineering of Donor- $\pi$ -Acceptor-Type Conjugated Microporous Polymers for Dual Effective Photocatalytic Production of Hydrogen and Hydrogen Peroxide

**Mohamed Gamal Mohamed,<sup>a,b,\*1</sup> Islam M. A. Mekhemer,<sup>b,c1</sup> Ahmed F. H. Selim,<sup>b,c1</sup> Andreas Katsamitros,<sup>d</sup> Dimitrios Tasis,<sup>d,e\*</sup> Abdul Basit,<sup>a</sup> Ho-Hsiu Chou,<sup>c,f,g,h\*</sup> and Shiao-Wei Kuo<sup>a,i\*</sup>**

<sup>a</sup>Department of Materials and Optoelectronic Science, Center for Functional Polymers and Supramolecular Materials, National Sun Yat-Sen University, Kaohsiung 804, Taiwan.

<sup>b</sup>Department of Chemistry, Faculty of Science, Assiut University, Assiut 71515, Egypt.

<sup>c</sup>Department of Chemical Engineering, National Tsing Hua University, Hsinchu 300044, Taiwan.

<sup>d</sup>Department of Chemistry, University of Ioannina, 45110 Ioannina, Greece.

<sup>e</sup>Institute of Materials Science and Computing, University Research Center of Ioannina (URCI), Ioannina 45110, Greece.

<sup>f</sup>Institute of Photonics Technologies, National Tsing Hua University, Hsinchu 30013, Taiwan.

<sup>g</sup>College of Semiconductor Research, National Tsing Hua University, Hsinchu 300044, Taiwan.

<sup>h</sup>Photonics Research Center, National Tsing Hua University, Hsinchu 300044, Taiwan.

<sup>i</sup>Department of Medicinal and Applied Chemistry, Kaohsiung Medical University, Kaohsiung 807, Taiwan.

### **Corresponding authors:**

E-mail: mgaml.eldin12@aun.edu.eg, mgamal.eldin12@yahoo.com (M. G. Mohamed), dtassis@uoi.gr (D. Tasis), hhchou@mx.nthu.edu.tw (H. H. Chou) and

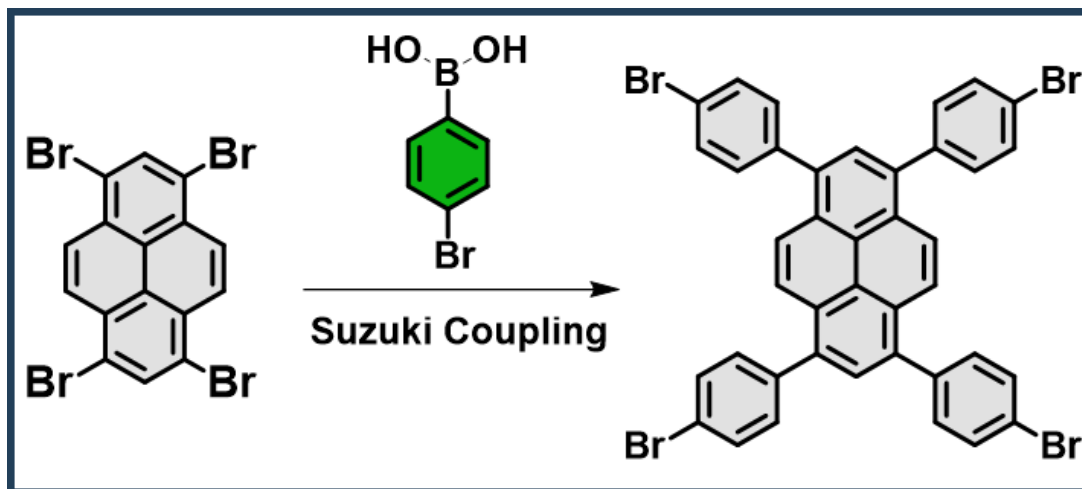
kuosw@faculty.nsysu.edu.tw (S. W. Kuo).

<sup>1</sup>These authors contributed equally to this work.

## Characterization

FTIR spectra were collected on a Bruker Tensor 27 FTIR spectrophotometer with a resolution of  $4\text{ cm}^{-1}$  by using the KBr disk method.  $^{13}\text{C}$  nuclear magnetic resonance (NMR) spectra were examined by using an INOVA 500 instrument with  $\text{DMSO-}d_6$  and  $\text{CDCl}_3$  as the solvents and TMS as the external standard. Chemical shifts are reported in parts per million (ppm). The thermal stabilities of the samples were performed by using a TG Q-50 thermogravimetric analyzer under a  $\text{N}_2$  atmosphere; the sample (ca. 5 mg) was put in a Pt cell with a heating rate of  $20\text{ }^\circ\text{C min}^{-1}$  from 100 to  $800\text{ }^\circ\text{C}$  under a  $\text{N}_2$  flow rate of  $60\text{ mL min}^{-1}$ . Solid-state  $^{13}\text{C}$  NMR was measured by JEOL JNM-LA300 spectrometer and a standard CPMAS probe at 75.577 MHz. The morphologies of the polymer network samples were examined by Field emission scanning electron microscopy (FE-SEM; JEOL JSM7610F). Surface area and porosity measurements of samples weighing approximately 40-60 mg were conducted using the BEL MasterTM/BEL simTM (version 3.0.0) apparatus. Nitrogen ( $\text{N}_2$ ) adsorption and desorption isotherms were generated by gradually exposing the samples to ultrahigh-purity  $\text{N}_2$  gas, reaching pressures of up to about 1 atmosphere, while maintaining a temperature of 77 K in a liquid nitrogen bath. Before these measurements, the samples underwent a degassing process at  $150\text{ }^\circ\text{C}$  for 8 h. The instrument's software was utilized to calculate surface parameters using the BET adsorption models. Furthermore, the pore size of the prepared samples was determined using the nonlocal density functional theory (NLDFT).

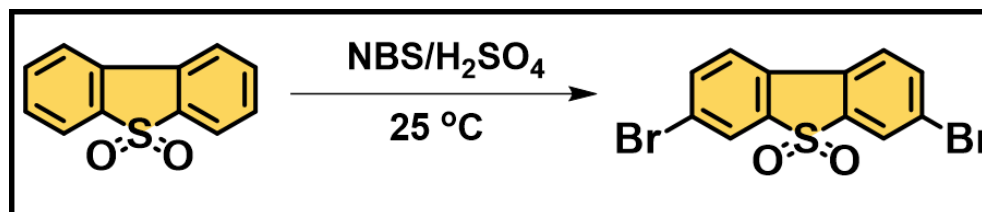
### Synthesis of 1,3,6,8-tetrakis(4-bromophenyl)pyrene [PyPh-4Br]



**Scheme S1.** Synthesis of PyPh-4Br.

In a mixture of 1,4-dioxane (100 mL) and H<sub>2</sub>O (40 mL), a reaction was carried out under vacuum using Pd(PPh<sub>3</sub>)<sub>4</sub> (0.8 g, 0.68 mmol), 4-bromophenylboronic acid (3.3 g, 22 mmol), K<sub>2</sub>CO<sub>3</sub> (4.3 g, 30.8 mmol), and Py-4Br (2.0 g, 3.8 mmol). The reaction mixture was then heated at 110 °C under a N<sub>2</sub> for 48 h. Upon completion, the resulting suspension was filtered, and the solid product was thoroughly washed with H<sub>2</sub>O, THF, and MeOH to afford a yellow powder [Scheme S1]. FTIR: 3038 (C–H aromatic), 1593 cm<sup>-1</sup>. HR-FD-MS: *m/z*: 822.90.

### Synthesis of 3,7-dibromodibenzo[b,d]thiophene 5,5-dioxide [DBZS-2Br]

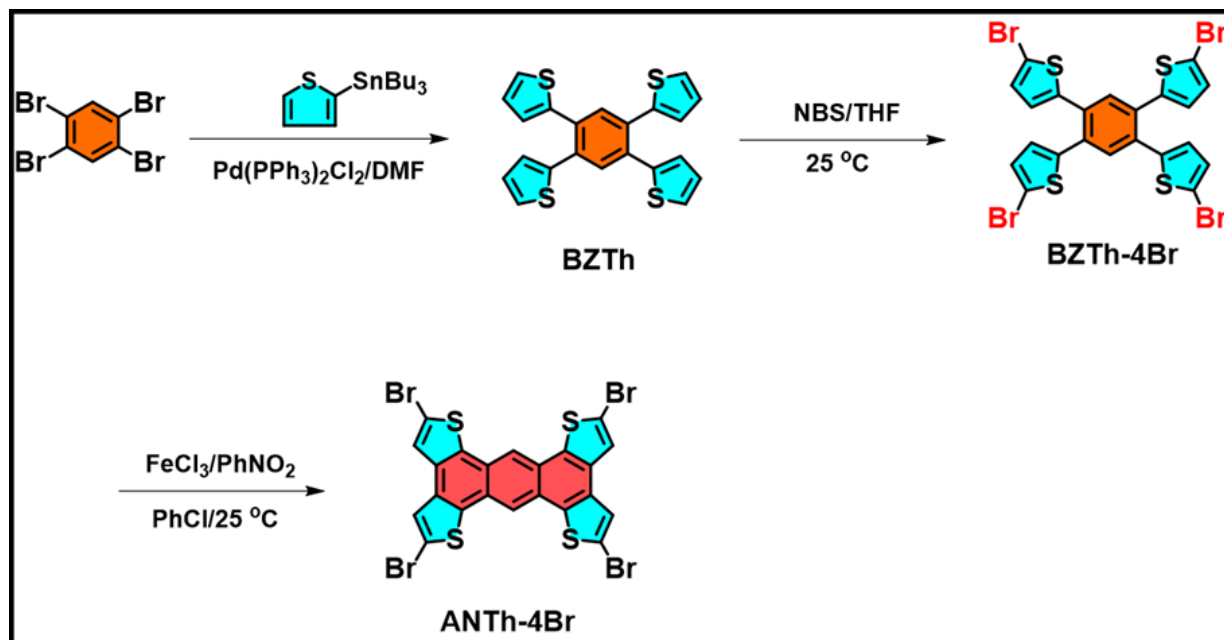


**Scheme S2.** Synthesis of DBZS-2Br.

### Synthesis of 3,7-dibromodibenzo[b,d]thiophene 5,5-dioxide [DBZS-2Br]

DBZS (6.0 g, 28 mmol) was dissolved in H<sub>2</sub>SO<sub>4</sub> (195 mL) at 0 °C. Subsequently, N-bromosuccinimide (NBS, 9.91 g, 56 mmol) was added portion-wise over time, and the reaction mixture was stirred at room temperature (25 °C) for 10 h. Upon completion, the reaction mixture was carefully poured into ice-cold water and extracted with CHCl<sub>3</sub>. The combined organic layers were dried over anhydrous MgSO<sub>4</sub>, filtered, and concentrated under reduced pressure. The crude product was purified by column chromatography using a hexane/DCM (1:1, v/v) eluent to afford DBZS-2Br as a white solid (8.0 g) [Scheme S2]. FTIR (Figure S1): 3083, 1303, 1169 (SO<sub>2</sub>) cm<sup>-1</sup>. <sup>1</sup>H NMR (Figure S2): 8.4, 8.2, 8.03 ppm.

### Synthesis of 2,5,9,12-tetrabromoanthra[1,2-b:4,3-b':5,6-b'':8,7-b''']tetrathiophene [ANTh-4Br]



Scheme S3. Synthesis of BZTh, BZTh-4Br and ANTh-4Br.

### **Photocatalytic H<sub>2</sub> evolution test**

The photocatalytic experiments were carried out in a 40 mL Pyrex reactor. The reactor was closed using a rubber septum. In a typical photocatalytic reaction, PyPh-DBZS CMP or ANTh-DBZS CMP (1 mg) was dispersed in 10 mL of the mixture of water/NMP (9/1 V/V) with 0.1M AA as the sacrificial electron donor. The suspension was purged with argon for 5 minutes to remove dissolved air. A 350 W Xenon lamp equipped with a cut-off filter (1000 W/m<sup>2</sup>,  $\lambda$ : 380-780 nm) was used as the light source. The light intensity of the Xe lamp was like that of the visible light region in standard 1 sun, as verified using a solar cell. Hydrogen samples were taken with a gas-tight syringe and injected into a Shimadzu GC-2014 gas chromatograph with Ar as carrier gas. Hydrogen was detected with a thermal conductivity detector, referring to standard hydrogen gases with known concentrations.

### **Quantum efficiency measurements**

In the AQY experiments, the catalyst solution was prepared by dispersing PyPh-DBZS CMP or ANTh-DBZS CMP (1 mg) in 10 mL of the mixture of water/NMP (9/1 V/V) with 0.1M AA as sacrificial electron donor and cocatalyst (2 wt% Pt). The suspension was illuminated with a 350 W Xe lamp with different bandpass filters (420 and 460 nm). The formation of hydrogen was quantified using a Shimadzu gas chromatograph (GC2014) operating at isothermal conditions using a semi-capillary column equipped with a thermal conductivity detector.

The AQY was calculated as follows:

$$\text{AQY} = [(\text{Number of evolved hydrogen molecules} \times 2) / \text{Number of incident photons}] \times 100\%$$

$$AQY = \frac{N_e}{N_p} \times 100\% = \frac{2 \times M \times N_A}{\frac{E_{total}}{E_{photon}}} \times 100\%$$

$$= \frac{2M \times N_A}{\frac{S \times P \times t}{h \times \frac{c}{\lambda}}} \times 100\% = \frac{2 \times M \times N_A \times h \times c}{S \times P \times t \times \lambda} \times 100\%$$

Where, M is the amount of H<sub>2</sub> molecules (mol), N<sub>A</sub> is Avogadro constant (6.022 × 10<sup>23</sup>/mol), h is the Planck constant (6.626 × 10<sup>-34</sup> J·s), c is the speed of light (3 × 10<sup>8</sup> m/s), S is the irradiation area (m<sup>2</sup>), P is the intensity of irradiation light (W/m<sup>2</sup>), t is the photoreaction time (s), λ is the wavelength of the monochromatic light (m).

### **Photocatalytic H<sub>2</sub>O<sub>2</sub> evolution**

For the preparation of the aqueous suspension, 30 mg of the PyPh-DBZS CMP or ANTh-DBZS CMPs photocatalysts was dispersed in a 100 ml solution of deionized water and ethanol as a sacrificial agent (1% of volume). The suspension was sonicated for 15 minutes under dark conditions and subsequently was purged with O<sub>2</sub> gas for another 15 minutes in a 250 ml reactor (Lenz, Germany). For the photocatalytic experiment, two 800 W visible light lamps were used as the light source. At specific time intervals (0, 0.5, 1, 2, and 3 hours), aliquots of 2 ml were collected from the reactor and filtered through a 0.22 μm filter. In a vial, 0.3 ml of the aforementioned filtrate was mixed with 3 ml of a 0.2 mM solution of Ce(SO<sub>4</sub>)<sub>2</sub> and 0.7 ml of deionized water. The concentration of produced H<sub>2</sub>O<sub>2</sub> was measured via the ceric sulphate titration method using a UV-Vis spectrophotometer. The concentration of evolving H<sub>2</sub>O<sub>2</sub> was measured through the absorbance of Ce<sup>4+</sup> at 316 nm and the use of the calibration curve. The yellow-colored Ce<sup>4+</sup> was transformed into colorless Ce<sup>3+</sup>, according to the following reaction



where C(H<sub>2</sub>O<sub>2</sub>) = ½ C(Ce<sup>4+</sup>).

The formation of hydrogen peroxide by two-electron oxygen reduction may take place either through a concerted or a stepwise mechanism. In the former case, the half-reaction has a potential of -5.18 eV (vs vacuum) (see Eq. 1). Alternatively, oxygen molecules may be reduced to superoxide radical species, which may be further reduced to hydrogen peroxide (Eq. 2 and 3). These half-reactions have a potential of -4.17 eV and -5.94 eV, respectively. As a parallel scenario, superoxide radicals may participate in a disproportionation scheme, giving rise to hydrogen peroxide molecules (Eq. 4). Besides the reductive approach, the peroxide may be formed via the participation of valence band holes, which demonstrate an oxidative character. The so-called sacrificial agent, water, may be converted to H<sub>2</sub>O<sub>2</sub> through a two-hole-mediated concerted reaction (Eq. 5, potential -6.26 eV). Alternatively, the process may take place through two consecutive steps (Eq. 6 and 7).”



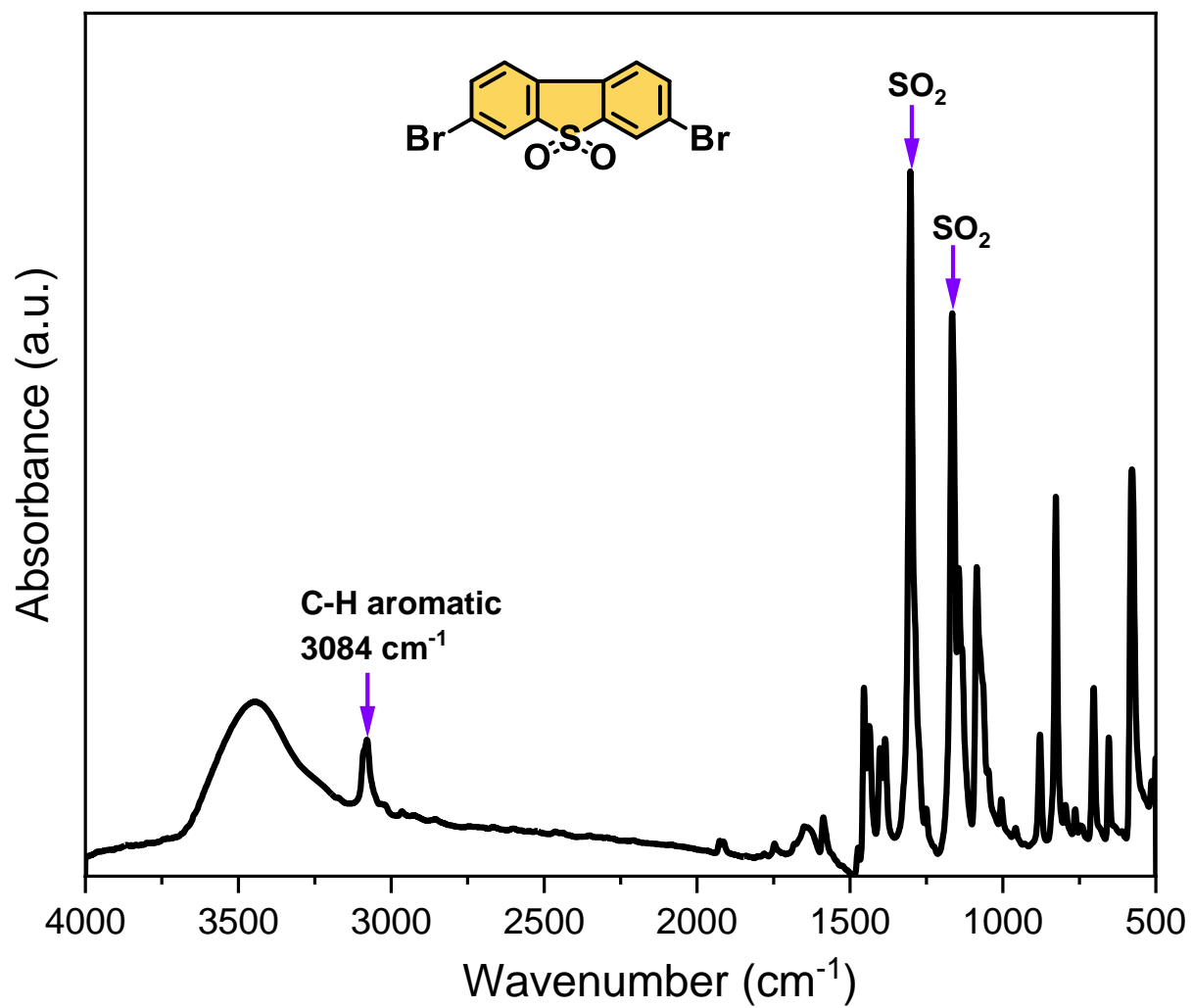


**Figure S1.** FTIR spectrum of DBZS-2Br.

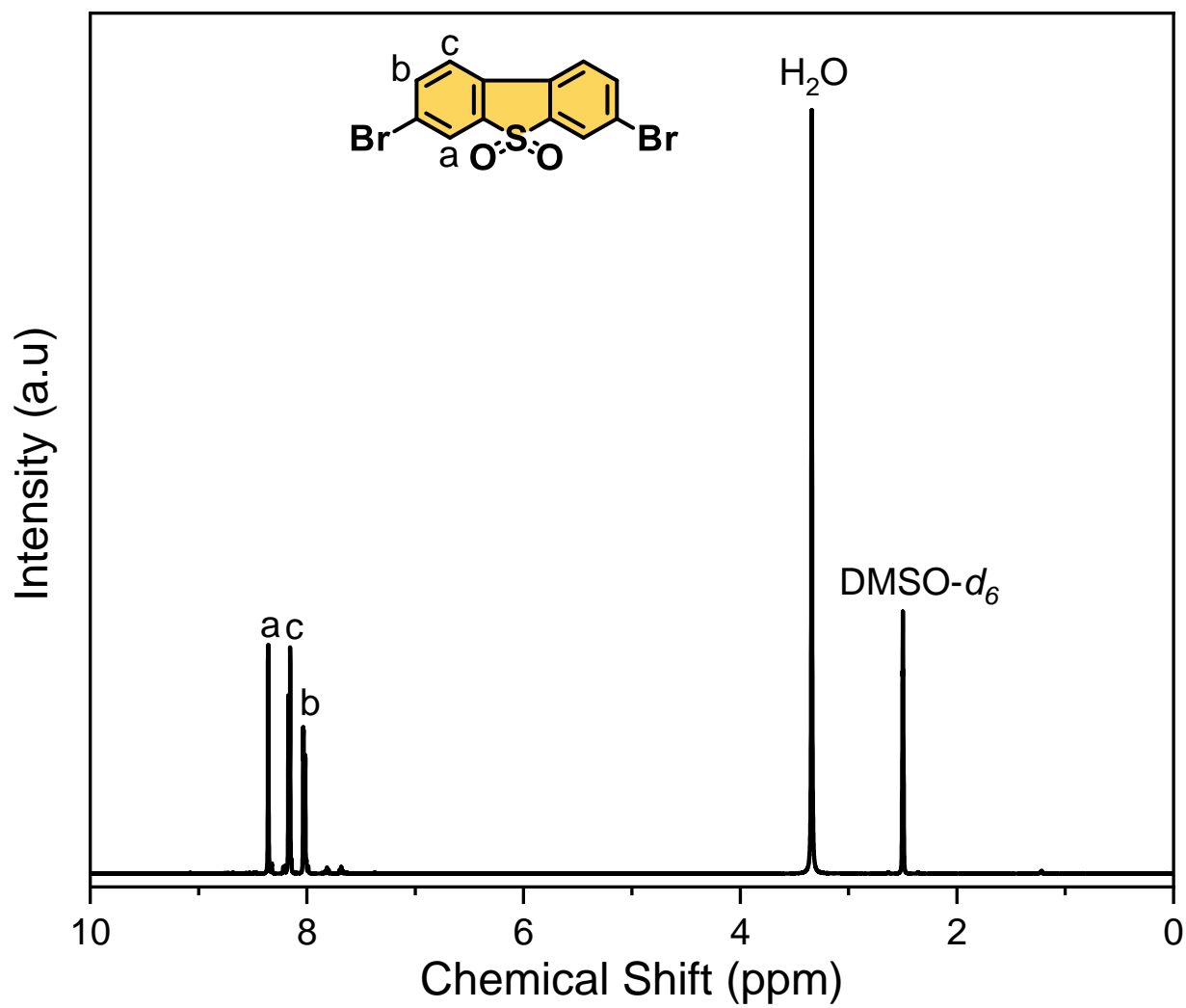


**Figure S2.**  $^1\text{H}$  NMR spectrum of DBZS-2Br.

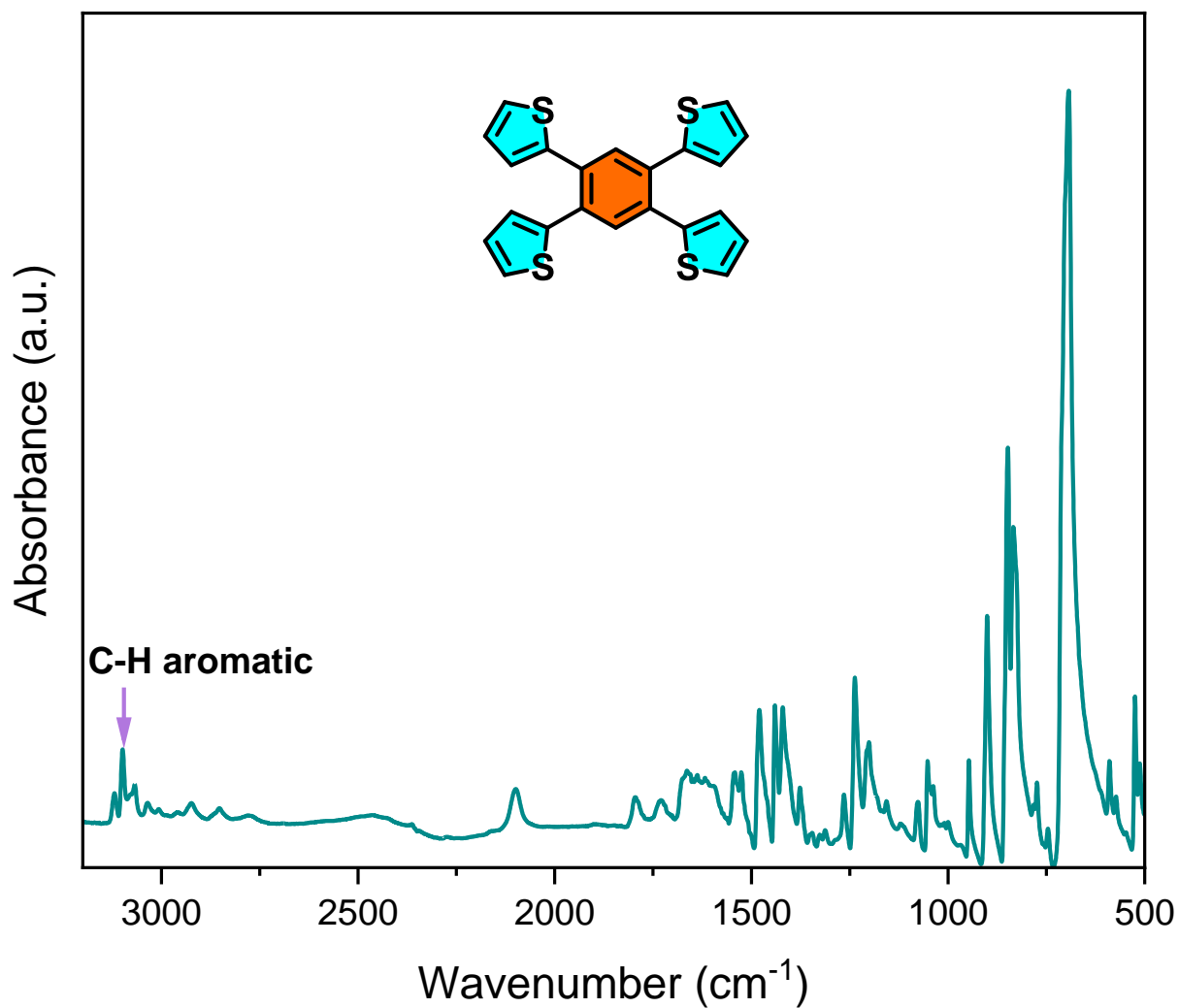


**Figure S3.** FTIR spectrum of BZTh.

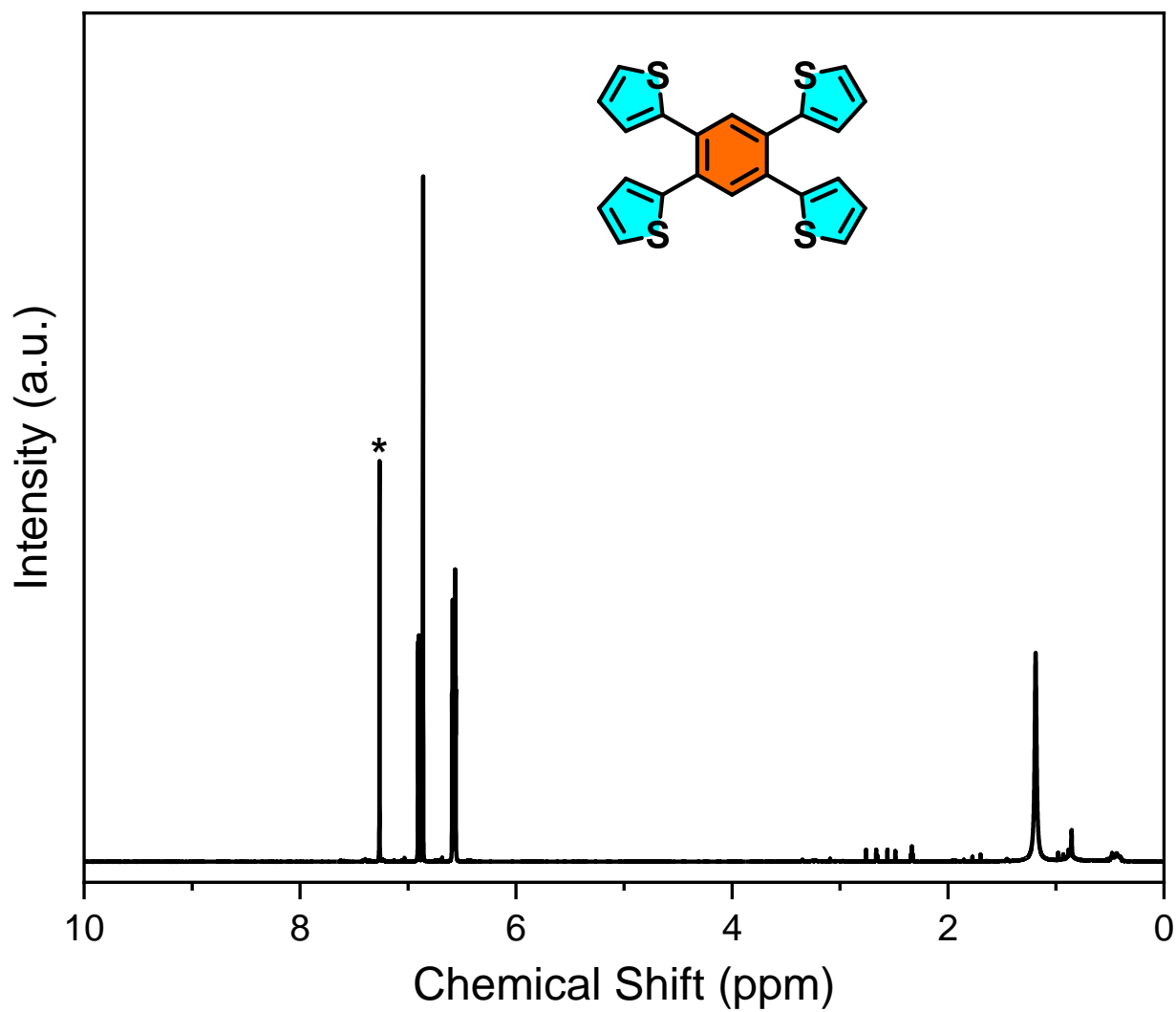


**Figure S4.**  $^1\text{H}$  NMR spectrum of BZTh.

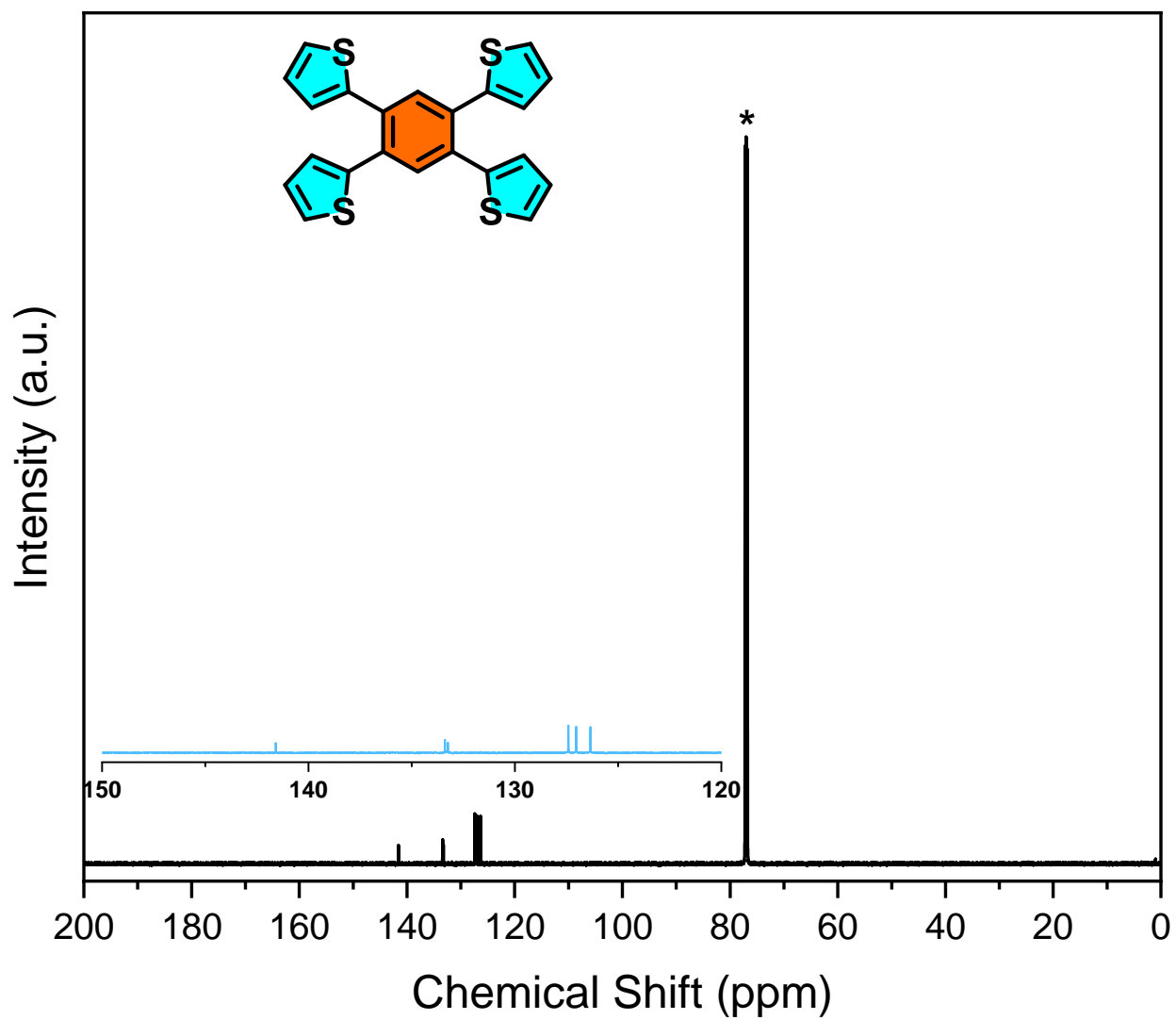


**Figure S5.**  $^{13}\text{C}$  NMR spectrum of BZTh.

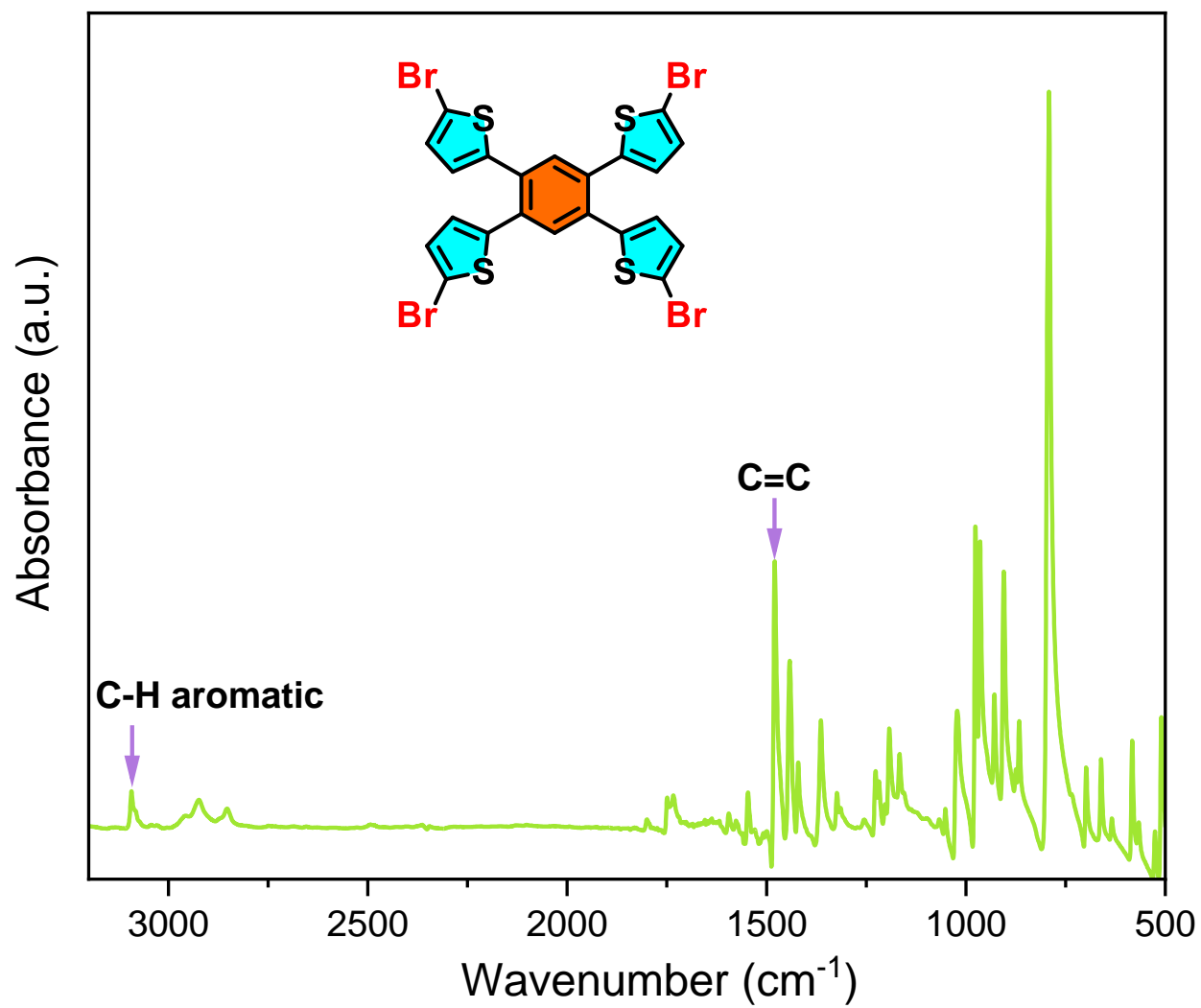


**Figure S6.** FTIR spectrum of BZTh-4Br.

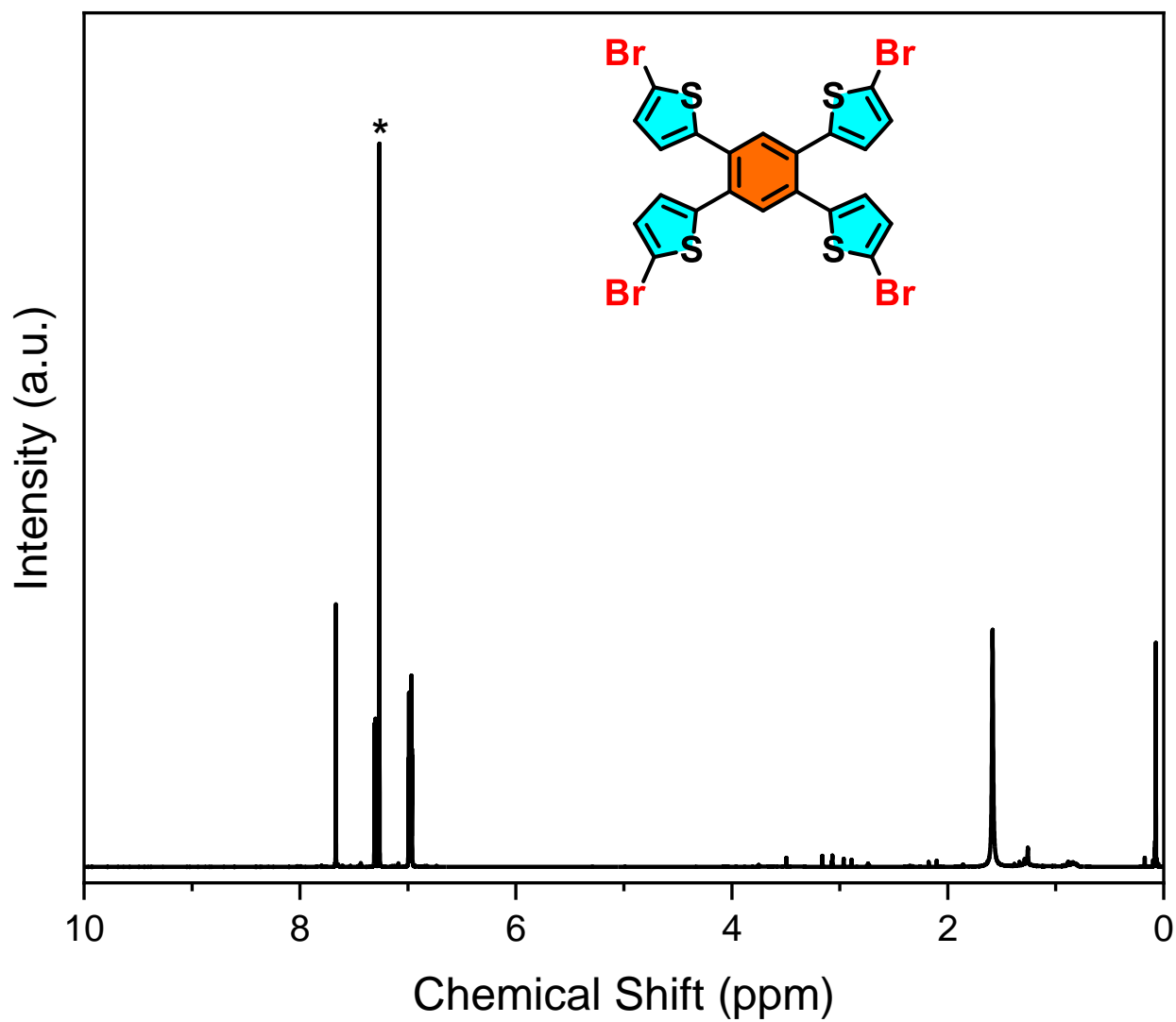


**Figure S7.**  $^1\text{H}$  NMR spectrum of BZTh-4Br.

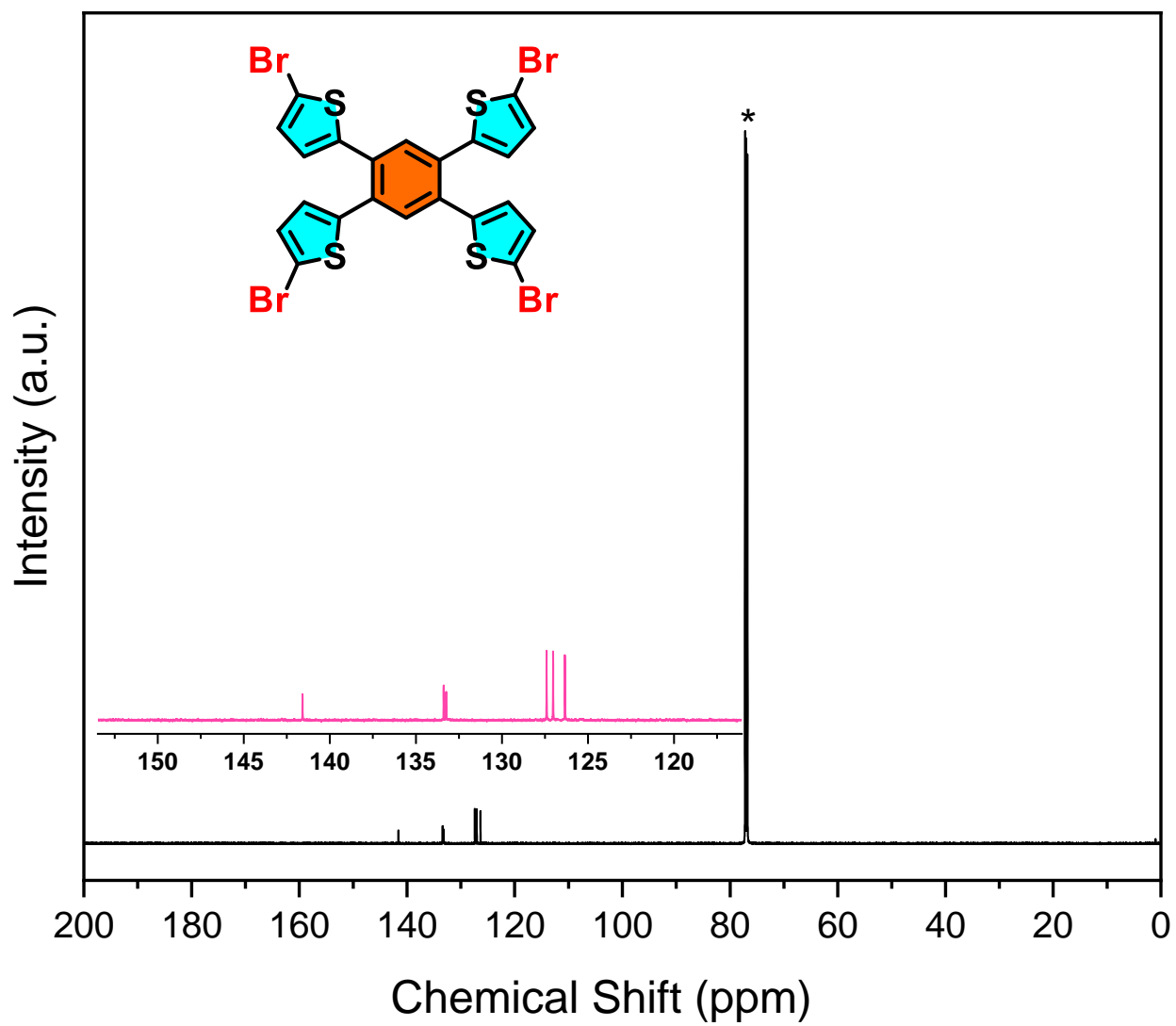
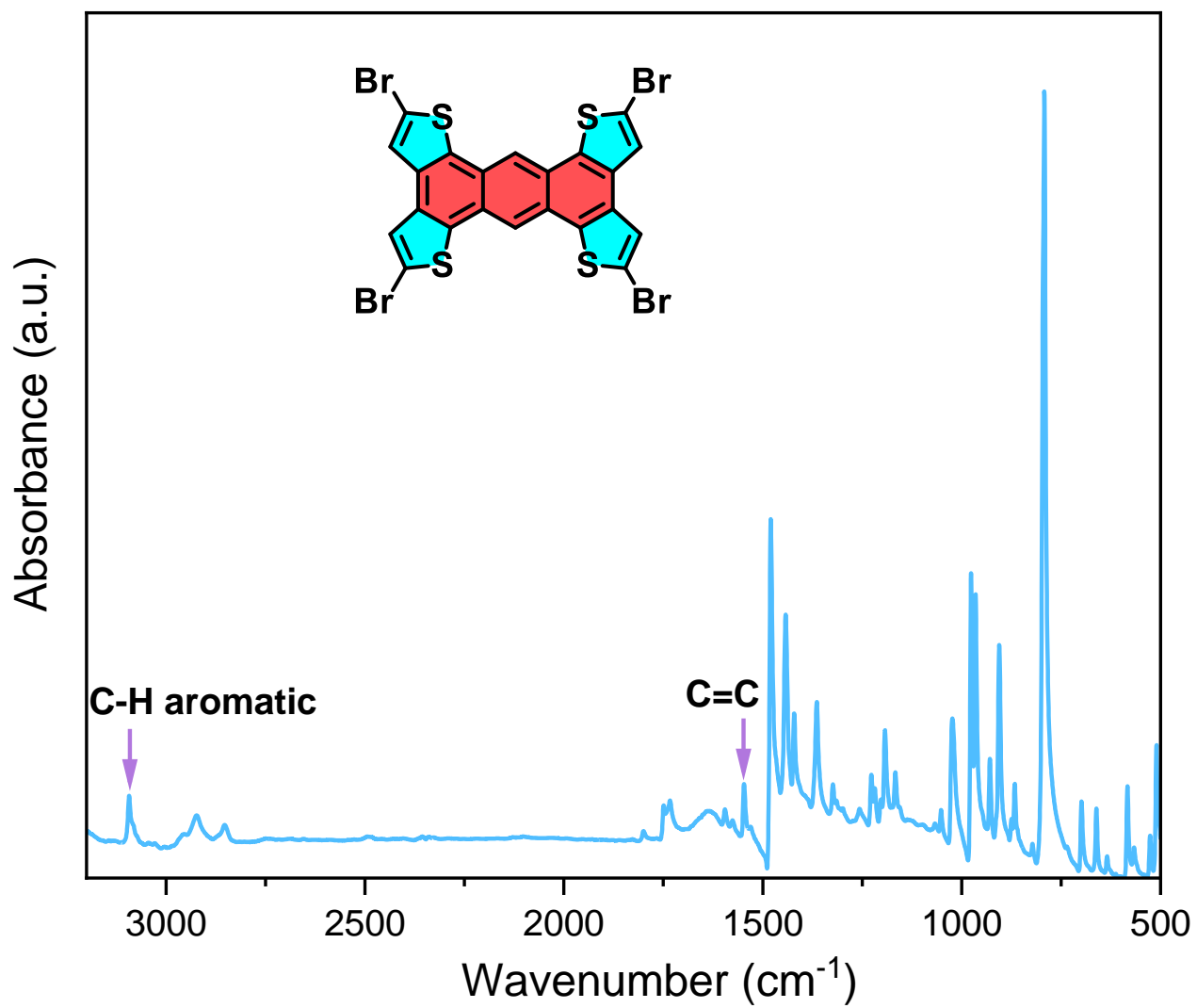
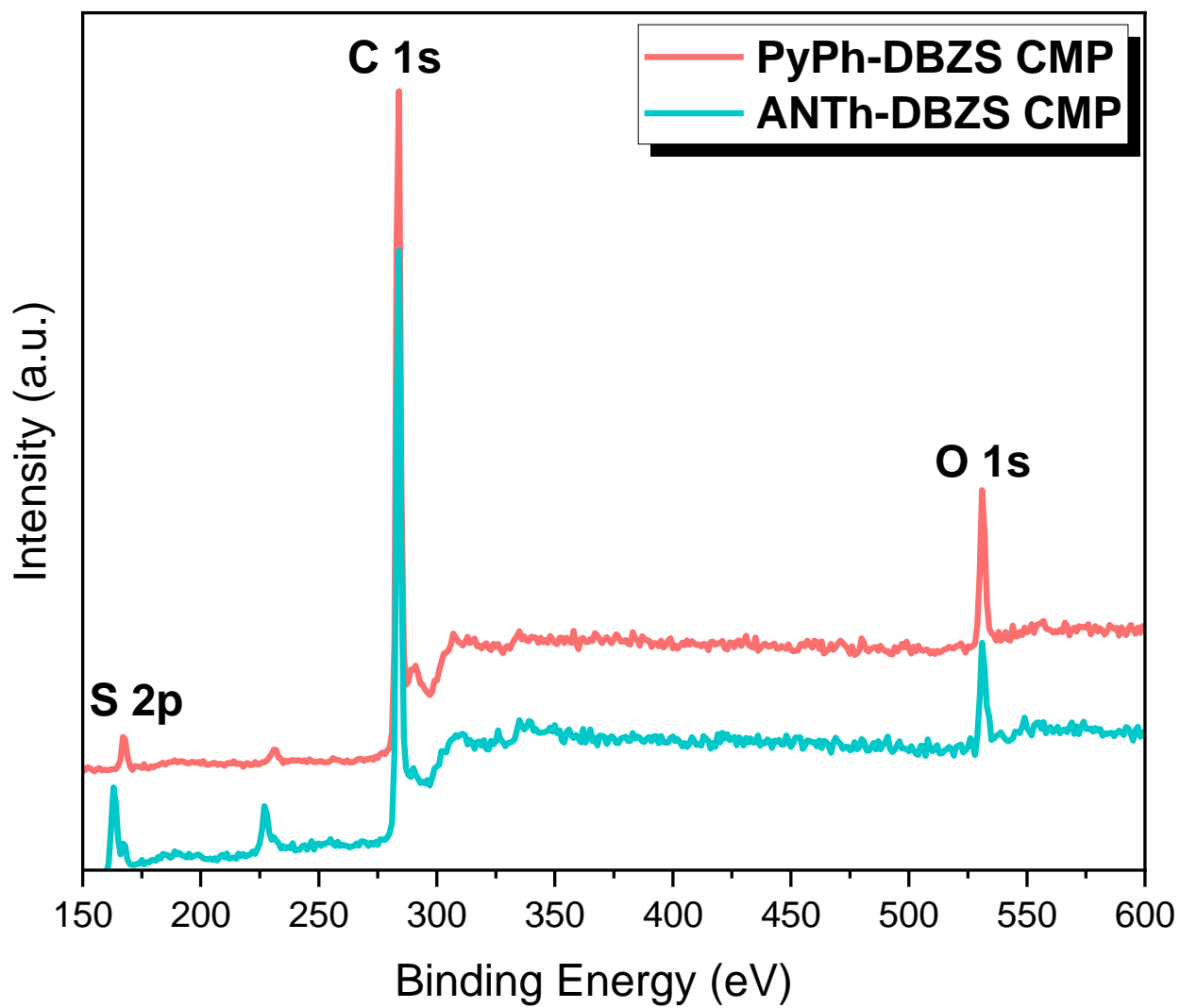


Figure S8.  $^{13}\text{C}$  NMR spectrum of BZTh-4Br



**Figure S9.** FTIR spectrum of ANTh-4Br.



**Figure S10.** High-resolution XPS (HR XPS) profiles of (a) PyPh-DBZS CMP and (b) ANTh-DBZS CMP.

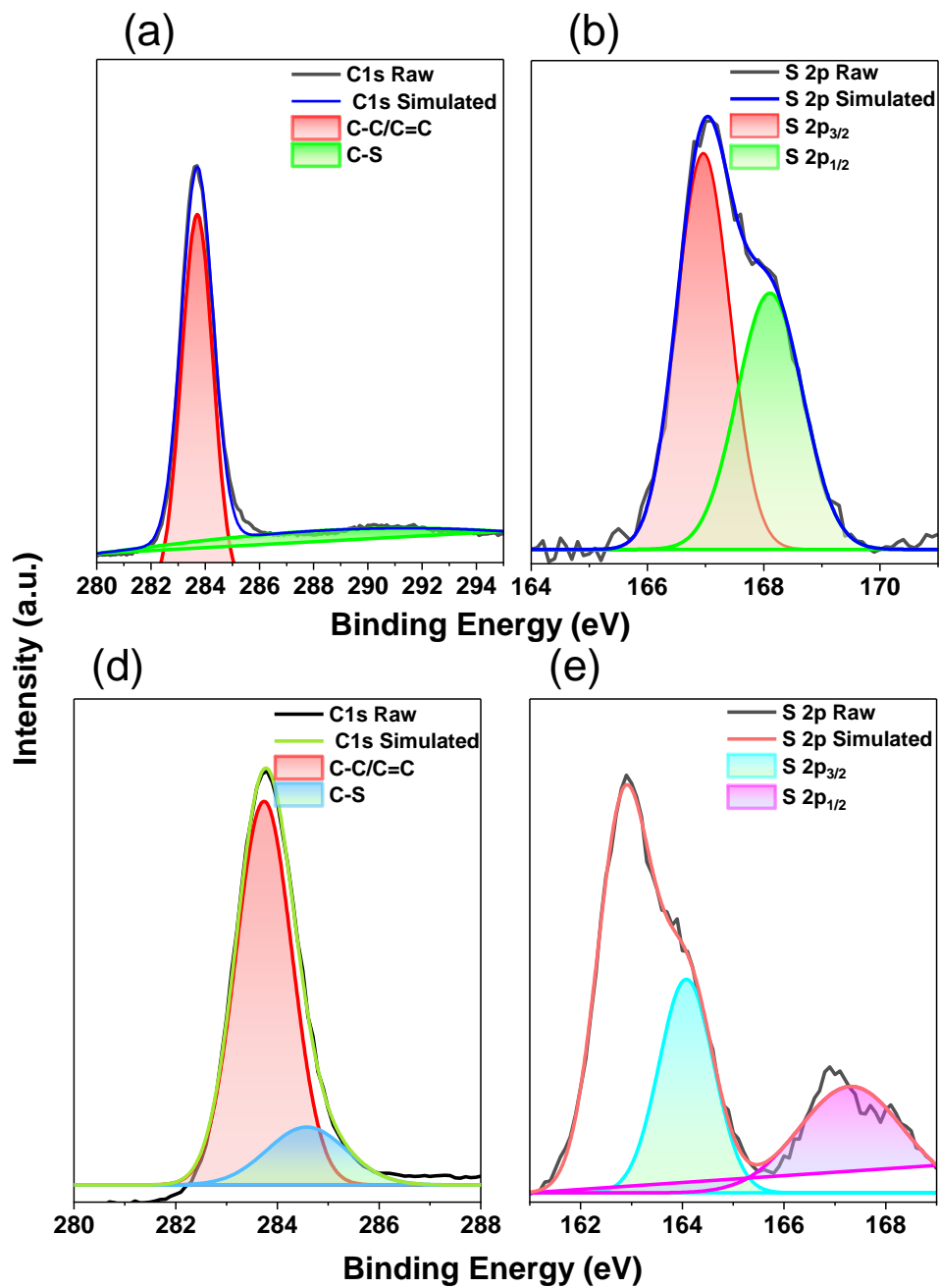


**Figure S11.** High-resolution XPS (HR XPS) fitting profiles of C 1s, and S 2p elements for (a, b) PyPh-DBZS CMP and (c, d) ANTh-DBZS CMP.

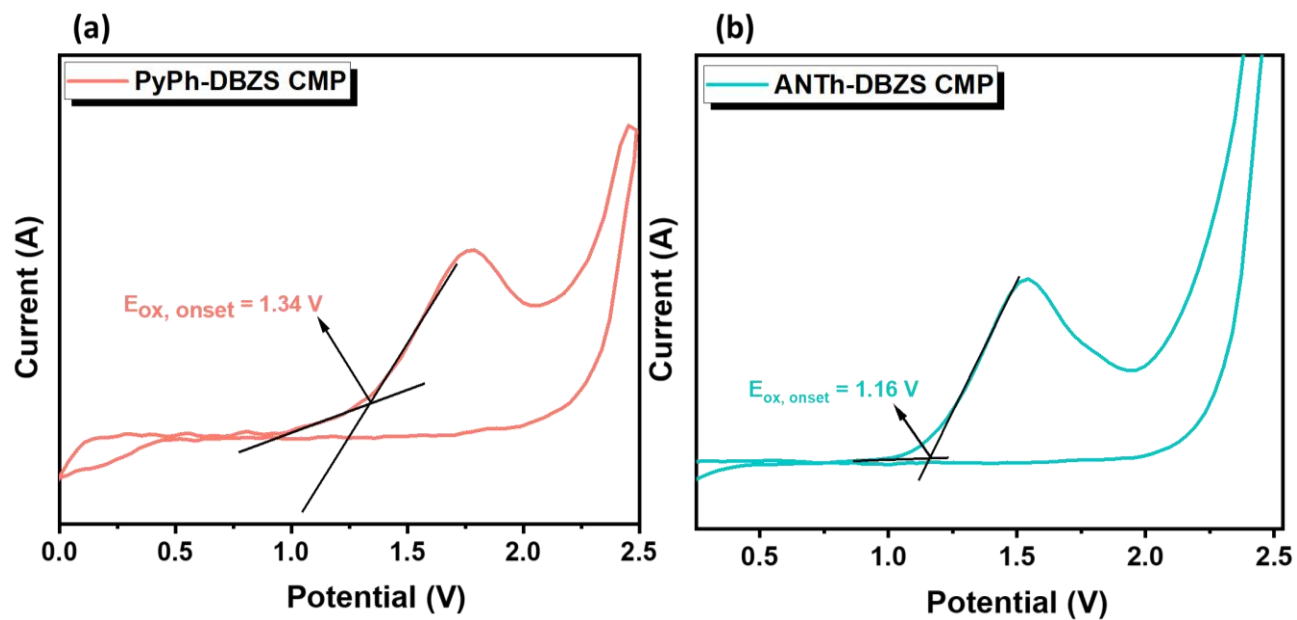


**Figure S12.** (a) and b) Onset potential of the first oxidation peak of Cyclic voltammetry for PyPh-DBZS CMP and ANTh-DBZS CMP using Ag/AgCl as a reference electrode based on the following equation ( $E\text{-HOMO} = E_{ox, onset} - E_{Ref} + 4.4$ ) eV,  $E_{Ref} = 0.159 + 0.059 \cdot \text{pH}$ ).

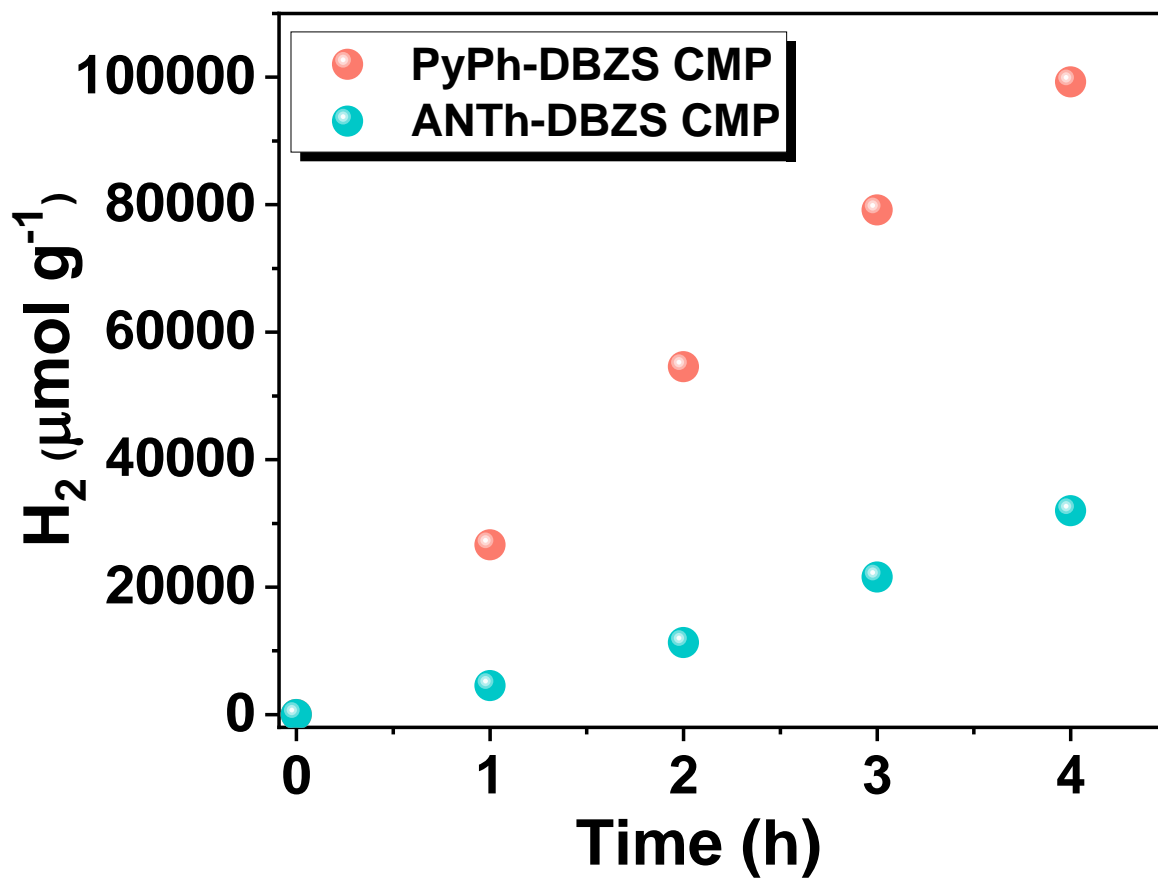


**Figure S13.** Time-dependent HER of PyPh-DBZS and ANTh-DBZS CMPs without Pt-loading.

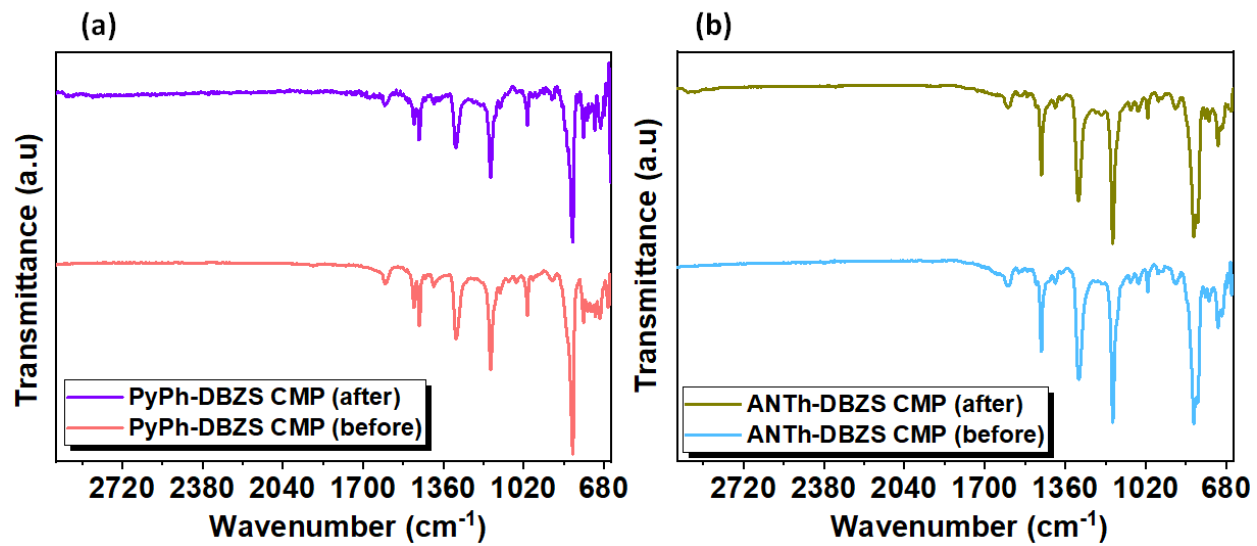


**Figure S14.** FTIR spectra before and after H<sub>2</sub> production reaction, (a) PyPh-DBZS CMP and (b) ANTh-DBZS CMP.

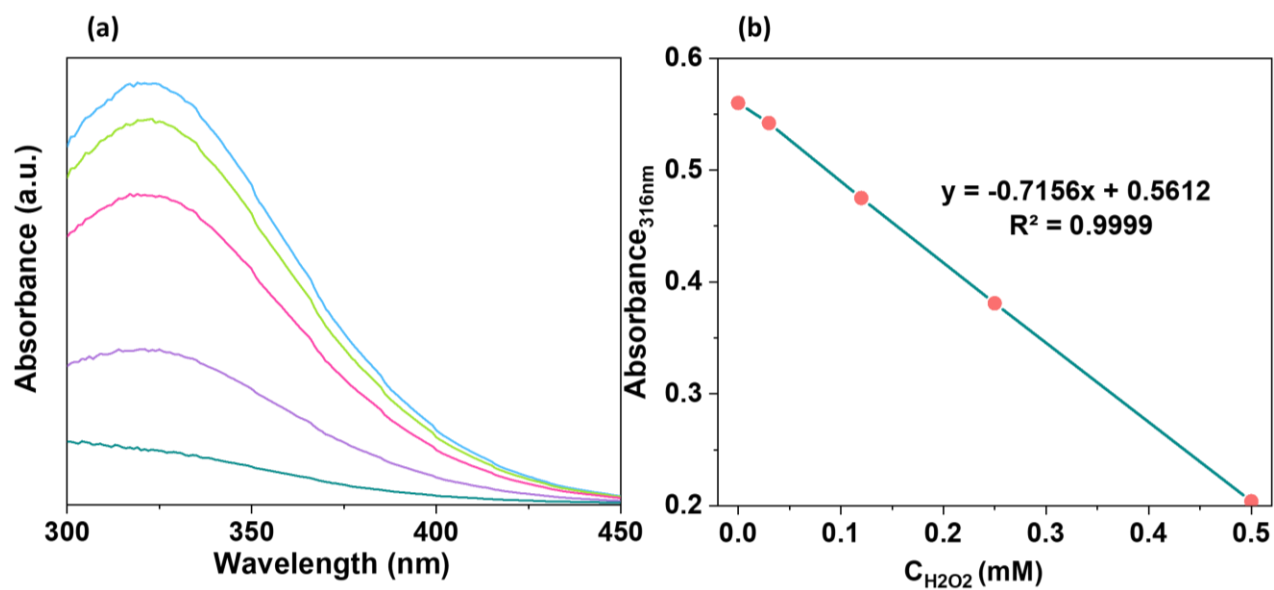


**Figure S15.** The H<sub>2</sub>O<sub>2</sub> generation was measured by Ce<sup>4+</sup> titration. The change of absorption intensity at  $\lambda_{\text{max}} = 316$  nm was measured by a UV-vis spectrometer. (b) The H<sub>2</sub>O<sub>2</sub> concentration-absorbance calibration curve.

**Table S1.** Elemental compositions of ANTh-DBZS CMP and PyPh-DBZS CMP as determined by X-ray photoelectron spectroscopy (XPS).

Sample	C (%)	S (%)	O (%)
ANTh-DBZS CMP	68.8	16.2	14.9
PyPh-DBZS CMP	86.2	2.6	11.1

**Table S2.** Summary of the fitted XPS data for C and S elements in ANTh-DBZS CMP and PyPh-DBZS CMP, as obtained from X-ray photoelectron spectroscopy (XPS) analysis.

Sample	C 1s		S 2p	
	C-C/C=C	C-S	S 2p <sub>3/2</sub>	S2p <sub>1/2</sub>
ANTh-DBZS CMP	69.9 %	30.1 %	64.2 %	35.5 %
PyPh-DBZS CMP	82.4 %	17.6 %	55.6 %	44.7 %

**Table S3.** Comparison of the photocatalytic hydrogen evolution performance of ANTh-DBZS CMP and PyPh-DBZS CMP with representative covalent organic frameworks (COFs), COF-based composites, conjugated microporous polymers (CMPs), polymer-based composites, and graphitic carbon nitride-based composites.

Photocatalyst	$\lambda$ (nm)	SDE	Co-cat.	HER ( $\mu\text{mol g}^{-1} \text{h}^{-1}$ )	AQY %	Ref.
PyPh-DBZS CMP	380-700 nm	AA	Pt (2 wt%)	133241	21.6 (at 420 nm)	This work
PyPh-DBZS CMP	380-700 nm	AA	Pt (2 wt%)	34791	5.6 (at 420 nm)	This work
FS-COF+WS5F	>420	AA	Pt (8 wt%)	16300	~7.2 (at 420 nm)	[S1]
g-C <sub>18</sub> N <sub>3</sub> -COF	>420	AA	Pt (3 wt%)	292	1.06 (at 420 nm)	[S2]
COP-64/TiO <sub>2</sub>	>420	MeOH	Pt (3 wt%)	15020	-	[S3]
TBN-TBN CMP	>420	AA	Pt (2 wt%)	8452	4.19 (at 420 nm)	[S4]
TBN-TBN-TPA CMP	>420	AA	Pt (2 wt%)	9800	5.07 (at 420 nm)	[S4]
TBN-BT CMP	>420	AA	Pt (2 wt%)	3060	0.57 (at 420 nm)	[S4]
COP-TP <sub>1:3</sub>	>420	TEOA	Pt (3 wt%)	4200	1.5 (at 420 nm)	[S5]
COP-TP <sub>1:3</sub>	>420	TEOA	Pt (3 wt%)	4200	0.5 (at 500 nm)	[S5]
DPBT-TP COP	>420	AA	Pt (7.5 wt%)	17,806	3.28 (at 420 nm)	[S6]
BpZn-COP	>420	TEOA	Pt (3 wt%)	162	-	[S7]
TiO <sub>2</sub> @BpZn-COP	>420	TEOA	-	1333	2.5 (at 420 nm)	[S7]
g-C <sub>40</sub> N <sub>3</sub> -COF	>420	TEOA	Pt (3 wt%)	4120	4.84 (at 420 nm)	[S8]
g-C <sub>54</sub> N <sub>6</sub> -COF	>420	TEOA	Pt (3 wt%)	2519	-	[S9]
ter-CTF-0.7	>420	TEOA	Pt (2 wt%)	19300	22.8 (at 420 nm)	[S10]
ZnPor-DETH-COF	>400	TEOA	Pt (8 wt%)	413	0.063 (at 450 nm)	[S11]
TtaTfa	>420	AA	Pt (8 wt%)	20700	1.43 (at 450 nm)	[S12]
CdS-COF	>420	LA	Pt (0.5 wt%)	3678	4.2 (at 420 nm)	[S13]
Pt-PVP-TP-COF	>420	AA	Pt	8420	0.4	[S14]

			(6 wt%)		(at 475 nm)	
CNS-COF	>420	TEOA	Pt (3 wt%)	46400	31.8 (at 425 nm)	[S15]
30%PEG@BT-COF	>420	AA	Pt (3.5 wt%)	11140	11.2 (at 420 nm)	[S16]
CYANO-CON	>420	AA	Pt (1 wt%)	134200	82.6 (at 450 nm)	[S17]
PyPz-COF	>420	AA	Pt	7542	-	[S18]
TAPFy-PhI COF	>420	AA	Pt	1763	-	[S19]
Py-DNII-COF	>420	AA	Pt (2 wt%)	625	-	[S20]
TPET-TTh CMP	>420	AA	Pt (1.5 wt%)	4600	2.8 (at 450 nm)	[S21]
PyT-TTh CMP	>420	AA	Pt (1.5 wt%)	18533	5.3 (at 450 nm)	[S21]

## References

- [S1] X. Wang, L. Chen, S. Y. Chong, M. A. Little, Y. Wu, W. H. Zhu, R. Clowes, Y. Yan, M. A. Zwijnenburg and R. S. Sprick. Sulfone-containing covalent organic frameworks for photocatalytic hydrogen evolution from water. *Nat. Chem.* 2018, **10**, 1180–1189.
- [S2] S. Wei, F. Zhang, W. Zhang, P. Qiang, K. Yu, X. Fu, D. Wu, S. Bi and F. Zhang. Semiconducting 2D triazine-cored covalent organic frameworks with unsubstituted olefin linkages. *J. Am. Chem. Soc.* 2019, **141**, 14272–14279.
- [S3] Q. Yang, P. Peng and Z. Xiang. Covalent organic polymer modified TiO<sub>2</sub> nanosheets as highly efficient photocatalysts for hydrogen generation. *Chem. Eng. Sci.* 2017, **162**, 33–40.
- [S4] S. Y. Chang, A. M. Elewa, M. G. Mohamed, I. M. A. Mekhemer, M. M. Samy, K. Zhang, H. H. Chou and S. W. Kuo. Rational design and synthesis of bifunctional Dibenzo[g,p]chrysene-based conjugated microporous polymers for energy storage and visible light-driven photocatalytic hydrogen evolution. *Mater. Today Chem.* 2023, **33**, 101680.

- [S5] Y. Liu, Z. Liao, X. Ma and Z. Xiang. Ultrastable and efficient visible-light-driven hydrogen production based on donor–acceptor copolymerized covalent organic polymer. *ACS Appl. Mater. Interfaces* 2018, **10**, 30698–30705.
- [S6] A. M. Elewa, M. H. Elsayed, A. F. M. El-Mahdy, C. L. Chang, L. Y. Ting, W. C. Lin, C. Y. Lu and H. H. Chou. Triptycene-based discontinuously-conjugated covalent organic polymer photocatalysts for visible-light-driven hydrogen evolution from water. *Appl. Catal. B Environ.* 2021, **285**, 119802.
- [S7] J. Chen, X. Tao, L. Tao, H. Li, C. Li, X. Wang, C. Li, R. Li and Q. Yang. Novel conjugated organic polymers as candidates for visible-light-driven photocatalytic hydrogen production. *Appl. Catal. B Environ.* 2019, **241**, 461–470.
- [S8] S. Bi, C. Yang, W. Zhang, J. Xu, L. Liu, D. Wu, X. Wang, Y. Han, Q. Liang and F. Zhang. Two-dimensional semiconducting covalent organic frameworks via condensation at arylmethyl carbon atoms. *Nat. Commun.* 2019, **10**, 2467.
- [S9] J. Xu, C. Yang, S. Bi, W. Wang, Y. He, D. Wu, Q. Liang, X. Wang and F. Zhang. Vinylene-linked covalent organic frameworks (COFs) with symmetry-tuned polarity and photocatalytic activity. *Angew. Chem. Int. Ed.* 2020, **132**, 24053–24061.
- [S10] L. Guo, Y. Niu, S. Razzaque, B. Tan and S. Jin. Design of D–A1–A2 covalent triazine frameworks via copolymerization for photocatalytic hydrogen evolution. *ACS Catal.* 2019, **9**, 9438–9445.
- [S11] Z. Mi, T. Zhou, W. Weng, J. Unruangsri, K. Hu, W. Yang, C. Wang, K.A.I. Zhang and J. Guo. Covalent Organic Frameworks Enabling Site Isolation of Viologen-Derived Electron-Transfer Mediators for Stable Photocatalytic Hydrogen Evolution. *Angew. Chem. Int. Ed.* **2021**, *133*, 9728–9735.

- [S12] J. Yang, A. Acharjya, M. Ye, J. Rabeah, S. Li, Z. Kochovski, S. Youk, J. Roeser, J. Grüneberg and C. Penschke. Protonated Imine-Linked Covalent Organic Frameworks for Photocatalytic Hydrogen Evolution. *Angew. Chemie Int. Ed.* 2021, **60**, 19797–19803.
- [S13] J. Thote, H. B. Aiyappa, A. Deshpande, D. Diaz, S. Kurungot and R. Banerjee. A Covalent Organic Framework–Cadmium Sulfide Hybrid as a Prototype Photocatalyst for Visible-Light-Driven Hydrogen Production. *Chem. Eur. J.* 2014, **20**, 15961–15965.
- [S14] J. Ming, A. Liu, J. Zhao, P. Zhang, H. Huang, H. Lin, Z. Xu, X. Zhang, X. Wang and J. Hofkens. Hot  $\pi$ -Electron Tunneling of Metal–Insulator–COF Nanostructures for Efficient Hydrogen Production. *Angew. Chem. Int. Ed.* 2019, **58**, 18290–18294.
- [S15] M. Luo, Q. Yang, W. Yang, J. Wang, F. He, K. Liu, H. Cao and H. Yan. Defects engineering leads to enhanced photocatalytic H<sub>2</sub> evolution on graphitic carbon nitride–covalent organic framework nanosheet composite. *Small* 2020, **16**, 2001100.
- [S16] T. Zhou, L. Wang, X. Huang, J. Unruangsri, H. Zhang, R. Wang, Q. Song, Q. Yang, W. Li and C. Wang. PEG-stabilized coaxial stacking of two-dimensional covalent organic frameworks for enhanced photocatalytic hydrogen evolution. *Nat. Commun.* 2021, **12**, 3934.
- [S17] C. Li, J. Liu, H. Li, K. Wu, J. Wang and Q. Yang. Covalent organic frameworks with high quantum efficiency in sacrificial photocatalytic hydrogen evolution. *Nat. Commun.* 2022, **13**, 2357.
- [S18] F. Wang, L. Yang, X. Wang, Y. Rong, L. Yang, C. Zhang, F. Yan and Q. Wang. Pyrazine-Functionalized Donor–Acceptor Covalent Organic Frameworks for Enhanced Photocatalytic H<sub>2</sub> Evolution with High Proton Transport. *Small* 2023, **19**, 2207421.

- [S19] G. Zhang, M. Zhao, L. Su, H. Yu, C. Wang, D. Sun and Y. Ding. Donor–acceptor covalent–organic frameworks based on phthalimide as an electron-deficient unit for efficient visible-light catalytic hydrogen evolution. *ACS Appl. Mater. Interfaces*, 2023, **15**, 20310–20316.
- [S20] I. M. A. Mekhemer, M. M. Elsenety, A. M. Elewa, K. D. G. Huynh, M. M. Samy, M. G. Mohamed, D. M. Dorrah, D. C. K. Hoang, A. F. Musa, S. W. Kuo and H. H. Chou. Push–pull–pull interactions of 2D imide–imine-based covalent organic framework to promote charge separation in photocatalytic hydrogen production. *J. Mater. Chem. A*, 2024, **12**, 10790-10798.
- [S21] S. U. Sharma, M. H. Elsayed, I. M.A. Mekhemer, T. S. Meng, H. H. Chou, S. W. Kuo and M. G. Mohamed. Rational design of pyrene and thienyltriazine-based conjugated microporous polymers for high-performance energy storage and visible-light photocatalytic hydrogen evolution from water. *Giant* 2024, **17**, 100217.